Published online 15 November 2012

Nucleic Acids Research, 2013, Vol. 41, No. 2 ***e41***
doi:10.1093/nar/gks1036

A versatile cis-blocking and trans-activation strategy for ribozyme characterization

Andrew B. Kennedy[1], Joe C. Liang[2] and Christina D. Smolke[1,*]

[1]Department of Bioengineering, Stanford University, 473 Via Ortega, MC 4201, Stanford, CA 94305 and [2]Division of Chemistry and Chemical Engineering, 1200 E. California Blvd., MC 210-41, California Institute of Technology, Pasadena, CA 91125, USA

Received June 9, 2012; Revised September 6, 2012; Accepted October 5, 2012

ABSTRACT

Synthetic RNA control devices that use ribozymes as gene-regulatory components have been applied to controlling cellular behaviors in response to environmental signals. Quantitative measurement of the *in vitro* cleavage rate constants associated with ribozyme-based devices is essential for advancing the molecular design and optimization of this class of gene-regulatory devices. One of the key challenges encountered in ribozyme characterization is the efficient generation of full-length RNA from *in vitro* transcription reactions, where conditions generally lead to significant ribozyme cleavage. Current methods for generating full-length ribozyme-encoding RNA rely on a trans-blocking strategy, which requires a laborious gel separation and extraction step. Here, we develop a simple two-step gel-free process including cis-blocking and trans-activation steps to support scalable generation of functional full-length ribozyme-encoding RNA. We demonstrate our strategy on various types of natural ribozymes and synthetic ribozyme devices, and the cleavage rate constants obtained for the RNA generated from our strategy are comparable with those generated through traditional methods. We further develop a rapid, label-free ribozyme cleavage assay based on surface plasmon resonance, which allows continuous, real-time monitoring of ribozyme cleavage. The surface plasmon resonance-based characterization assay will complement the versatile cis-blocking and trans-activation strategy to broadly advance our ability to characterize and engineer ribozyme-based devices.

INTRODUCTION

Synthetic biology is advancing the design of genetic circuits encoding desired functions (1). As the proper functioning of synthetic genetic circuits often relies on the precise control and tuning of key protein component levels, much effort in the field has focused on developing programmable gene-regulatory devices. One class of gene-regulatory device, so called RNA control devices, uses RNA molecules to link changes in molecular signals to gene expression events. Progress in the fields of RNA biology and engineering have allowed construction of RNA control devices through the assembly of natural or synthetic components that encode more basic functions, such as sensing, information transmission and actuation (2). Because ribozymes can exhibit activity independent of cell-specific machinery, RNA control devices that use ribozyme-based actuator components have been demonstrated in diverse organisms, spanning bacterial, yeast and mammalian systems, to regulate cellular behaviors in response to one or more environmental signals (3–6).

We recently described a modular ribozyme device platform based on the functional coupling of three distinct components: an actuator encoded by a hammerhead ribozyme (HHRz) from satellite RNA of tobacco ringspot virus (sTRSV), a sensor encoded by an RNA aptamer and an information transmitter encoded by a sequence capable of a programmed strand-displacement event (3) (Figure 1). The transmitter component directs the device to partition between two primary functional conformations, where the aptamer-folded conformation can bind the cognate ligand and be associated with the disruption or restoration of the ribozyme catalytic core to construct devices that increase or decrease gene expression, respectively, in response to input ligand. For example, synthetic ribozyme devices that respond to theophylline have been designed and used for various cellular engineering applications (3,4). The quantitative tuning

*To whom correspondence should be addressed. Tel: +1 650 721 6371; Fax: +1 650 721 6602; Email: csmolke@stanford.edu

The authors wish it to be known that, in their opinion, the first two authors should be regarded as joint First Authors.

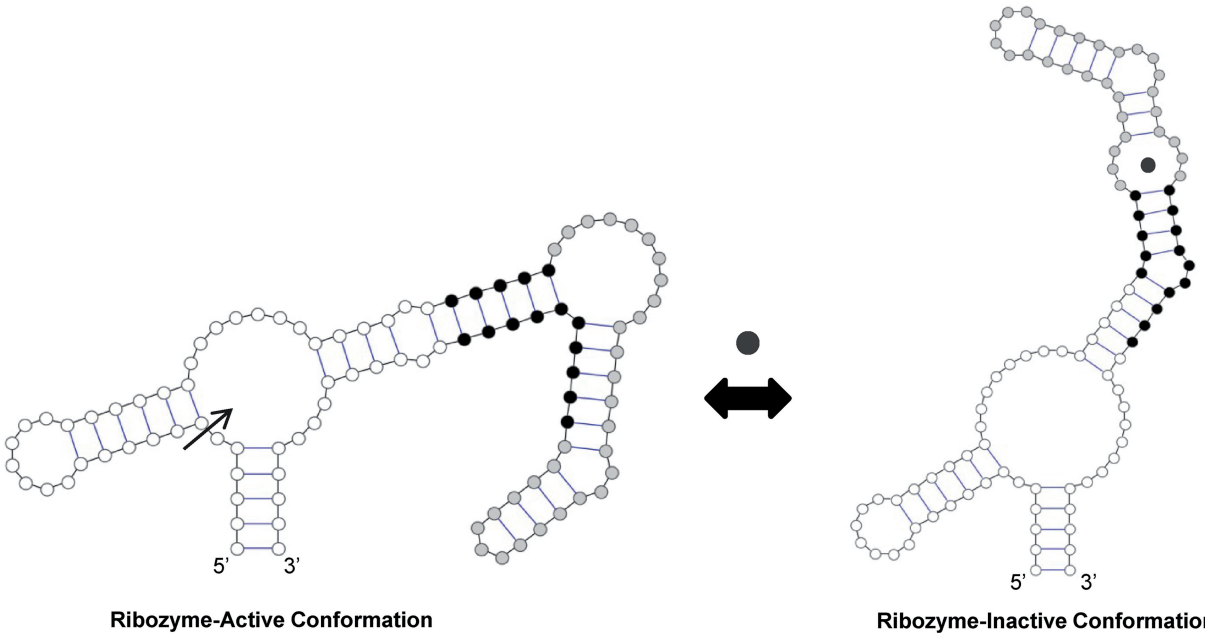

Figure 1. Modular composition and mechanism of a synthetic ligand-responsive ribozyme device. The ribozyme device is constructed by linking a RNA aptamer (indicated in grey) to a HHRz (indicated in white) through a transmitter sequence (indicated in black) that directs a strand-displacement event. The device can adopt two primary functional conformations, in which the ribozyme-active conformation is associated with either an aptamer-unformed or -formed conformation to construct a ribozyme device that upregulates or downregulates gene expression, respectively, in response to input ligand. The device depicted here favors the formation of the ribozyme-active conformation in the absence of the input ligand, thereby leading to self-cleavage and decreased gene expression. In the presence of the input ligand, binding of the ligand to the aptamer-formed conformation (i.e. ribozyme-inactive conformation) shifts the distribution to favor this conformation, resulting in no cleavage and increased gene expression. The arrow indicates the location of the cleavage site. All secondary structures were predicted by RNAstructure folding software (32) and rendered using VARNA software (33).

of the dynamic range of the regulatory device, which is determined by the gene-expression levels in the absence and presence of input ligand, has been demonstrated to be important for achieving effective control over phenotypic behaviors (4). Computational models of ribozyme devices have predicted that the ribozyme cleavage rate constant can have substantial impact on the gene-regulatory activities exhibited by a given device (7). Therefore, methods that allow the quantitative measurement of ribozyme cleavage rate constants of many sets of engineered RNA devices are essential to advance our understanding of the relationship between the *in vitro* cleavage rate constants and the corresponding *in vivo* gene-regulatory activities.

A key challenge in characterizing ribozyme cleavage rate constants is in the efficient generation of full-length RNA for ribozyme constructs, including natural ribozymes and synthetic ribozyme devices, by *in vitro* transcription. Typical transcription reactions require high $MgCl_2$ concentrations (~mM) to achieve sufficient yield, conditions at which most ribozyme constructs exhibit high cleavage activity, thereby resulting in low yield of full-length RNA for the subsequent kinetic analysis. In earlier approaches, researchers addressed this challenge by splitting the ribozyme sequence into enzyme and substrate strands such that the two strands were transcribed separately and annealed to generate a discontinuous ribozyme duplex (8–10). However, this strategy requires careful optimization of the experimental conditions to ensure that the measured cleavage rate constant is not affected by the association step between the two strands (11). More recently, researchers implemented a trans-blocking strategy to generate continuous ribozyme transcripts by including an antisense DNA oligonucleotide complementary to the ribozyme catalytic core in the transcription reactions to inhibit formation of the active structure. Full-length trans-blocked RNA is subsequently isolated through polyacrylamide gel electrophoresis (PAGE) under denaturing conditions, and the recovered RNA is renatured before performing the cleavage assay (8,12). Studies have shown that ~30% of the gel-purified full-length RNA is capable of cleaving during sample handling before initiating the cleavage assays, and ~50% of the remaining full-length RNA does not exhibit cleavage activity, where the loss of activity has been attributed to RNA misfolding (8). Therefore, a more efficient strategy to generate full-length ribozyme-encoding RNA is desired.

Ribozyme cleavage rate constants are typically measured through a gel electrophoretic separation method, which is convenient for detecting nucleic acids of different sizes (11,12). The cleavage reaction is initiated by the addition of $MgCl_2$ to radiolabeled full-length RNA and quenched at different time points. The cleaved and uncleaved strands in the quenched samples are resolved by denaturing PAGE to determine the fraction of RNA cleaved as a function of time, which are fit to a first-order exponential equation to ultimately obtain the cleavage rate constant. Because the gel-based ribozyme cleavage

assay is discontinuous, several time points are required in the initial and final phases of the reaction for proper analysis, thereby making the gel-based assay a time-consuming process. A continuous ribozyme cleavage assay based on the intramolecular fluorescence resonance energy transfer has been developed and applied to characterize ribozyme cleavage rate constants (13,14). However, the fluorescence resonance energy transfer-based cleavage assay requires labeling of RNA molecules with appropriate fluorophores and has only been applied to the characterization of discontinuous ribozyme duplexes.

Advances in biosensor technologies have led to the development of the Biacore platform based on surface plasmon resonance (SPR) for real-time detection of biomolecular interactions (15). The Biacore platform uses a sensor surface modified with one molecule and measures the refractive index change, which is associated with the local mass density change, owing to the association or dissociation of another molecule in solution. The refractive index change is converted into a SPR signal, which is expressed in resonance units (RU), and fit to a mathematical model to acquire thermodynamic and kinetic binding parameters. The Biacore platform requires no labeling of molecules, consumes little sample and is highly automated, thus making it an attractive tool for developing novel ribozyme characterization strategies.

In this work, we developed a simple gel-free strategy that allows efficient generation of full-length RNA sequences for diverse ribozyme constructs. Our strategy is inspired by an earlier structural study of the natural hepatitis delta virus (HDV) ribozyme (16). In the HDV RNA genome, the sequence immediately upstream of the HDV ribozyme cleavage site inhibits cleavage by hybridizing to part of the ribozyme, and the cleavage activity of the inhibited HDV ribozyme is rescued by the addition of a synthetic antisense oligomer, which sequesters the natural cis-blocking sequence through hybridization. We developed a similar two-step process, which can be adapted to different ribozymes. In the first blocking step, we designed an RNA sequence that was directly incorporated into the target transcript to co-transcriptionally inhibit the formation of the ribozyme-active conformations. In the second activation step, we designed a trans-acting DNA competing strand to restore the catalytic activity of the blocked RNA through a rapid toehold-mediated strand-displacement reaction. We demonstrated our two-step strategy to generate functional continuous RNA sequences for various types of natural ribozymes and synthetic ribozyme devices and observed high blocking and activation efficiencies up to ~97% and ~89%, respectively. The results from gel-based ribozyme cleavage assays validate that the RNA generated through our two-step strategy exhibit similar kinetics as those generated through traditional trans-blocking methods. Lastly, we developed a label-free, real-time, continuous SPR-based ribozyme cleavage assay. Our results suggest that the SPR-based cleavage assay can provide a rapid assessment of ribozyme cleavage activity under varying reaction conditions, thereby providing a powerful tool for complementing the traditional gel-based assay method.

MATERIALS AND METHODS

Preparation of DNA templates for T7 transcription reaction

DNA synthesis was performed by Integrated DNA Technologies (Coralville, IA) or the Protein and Nucleic Acid Facility (Stanford, CA). PCR products were used as the DNA templates for *in vitro* T7 transcription reactions. For the cis-blocked ribozyme constructs, PCR products were amplified from DNA templates using the forward primer T7-fwd (5′-TTCTAATACGACTCACTATAGG) and the corresponding reverse primer, which is specific to each construct (Supplementary Table S1).

Generation of full-length RNA through the cis-blocking strategy

A total of 1–2 μg of PCR product was transcribed in a 25 μl reaction, consisting of the following components: 1× RNA Pol Reaction Buffer (New England Biolabs, Ipswich, MA), 2.5 mM of each rNTP, 1 μl RNaseOUT (Invitrogen, Carlsbad, CA), 10 mM $MgCl_2$, 1 μl T7 RNA Polymerase (New England Biolabs) and 0.5 μCi α-^{32}P-GTP (MP Biomedicals, Solon, OH). The RNA concentration was estimated by performing a parallel cold (without radioactivity) transcription reaction. After incubation at 37°C for 2 h, NucAway Spin Columns (Ambion, Austin, TX) were used to remove unincorporated nucleotides from the transcription reactions according to manufacturer's instructions. The transcription products were purified with the RNA Clean and Concentrator™-5 (Zymo Research, Irvine, CA) kit according to manufacturer's instructions.

Gel-based ribozyme cleavage assays

All gel-based ribozyme cleavage assays were performed in a physiologically relevant reaction buffer (50 μl) composed of 500 μM $MgCl_2$, 100 mM NaCl and 50 mM Tris-HCl (pH 7.5) at 37°C unless otherwise specified. In the reaction volume, 75 nM of full-length RNA generated from the cis-blocking strategy was first incubated with 2.5 μM DNA activator strand (5′-AAACAACTTTGTTT GTTTCCCCC), which is ordered from Integrated DNA Technologies as an oligonucleotide with standard desalting, for 2 min to activate the blocked RNA. Full-length RNA generated from the trans-blocking strategy was incubated at 95°C for 5 min, cooled at a rate of −1.3°C/min to 37°C, and held at 37°C for 10 min to allow equilibration of secondary structure. A zero time-point aliquot was taken before initiating the self-cleavage reaction with the addition of $MgCl_2$. Reactions were quenched at specified time points with addition of 3 volumes of RNA stop/load buffer (95% formamide, 30 mM EDTA, 0.25% bromophenol blue, 0.25% xylene cyanol) on ice. Samples were heated to 95°C for 5 min, snap cooled on ice for 5 min and size-fractionated on a denaturing (8.3 M Urea) 10% polyacrylamide gel at 25 W for 45–60 min. Gels were exposed overnight on a phosphor screen and imaged on a FX Molecular Imager (Bio-Rad, Hercules, CA). The relative levels of the full-length transcript and cleaved products were determined by phosphorimaging analysis.

The blocking and activation efficiencies of the cis-blocked ribozyme constructs were determined by the fractions of the uncleaved RNA after the transcription reaction and the fractions of the cleaved blocked RNA at the end of incubation with DNA activator and $MgCl_2$, respectively. To determine cleavage rate constants, the cleaved product fraction at each time point (F_t) was fit to the single exponential equation $F_t = F_0 + (F_\infty - F_0) \times (1 - e^{-kt})$ using Prism 5 (GraphPad), where F_0 and F_∞ are the fractions cleaved before the start of the reaction and at the reaction endpoint, respectively, and k is the first-order rate constant of self-cleavage. All reported cleavage rate constants are the mean of at least three independent experiments.

Biacore sensor chip surface generation

Biosensor experiments were performed on a Biacore X100 instrument (Biacore, Uppsala, Sweden). A CM5 sensor chip (Biacore) was docked in the Biacore X100 and equilibrated with HBS-N buffer at 25°C. The DNA activator strand (5′-AAACAACTTTGTTTGTTTCCCCC-/AmMO/), with an amino modification on its 3′ end, was immobilized to the chip surface via standard amine-coupling chemistry. Briefly, the carboxymethyl surface of the CM5 chip was activated for 7 min at a flow rate of 5 µl/min using a 1:1 volume ratio of 0.4 M 1-ethyl-3-(3-dimethylaminopropyl) carbodiimide (Biacore) and 0.1 M N-hydroxysuccinimide (Biacore). A molar ratio of 1:60 of DNA activator to cetyl trimethylammonium bromide (Amresco, Solon, OH) was diluted in 10 mM HEPES buffer (Sigma, St. Louis, MO) to a final concentration of 10 µM and 0.6 mM, respectively, and injected over the activated surface for 10 min at a flow rate of 5 µl/min. Excess activated groups were blocked by an injection of 1 M ethanolamine (Biacore), pH 8.5, for 7 min at a flow rate of 5 µl/min. The immobilization reaction was performed on both flow cells (FC1, FC2), where FC1 was used as a reference cell to correct for bulk refractive index changes, matrix effects, non-specific binding, injection noise and baseline drift (17). Approximately 1600 RU of the activator strand was immobilized using this protocol.

Label-free SPR-based ribozyme cleavage assays

Full-length RNA was prepared as previously described for the cis-blocking strategy without the addition of the radiolabeled nucleotide. The Biacore X100 instrument was equilibrated with the physiologically relevant reaction buffer at 37°C unless otherwise specified before all ribozyme cleavage assays. The SPR baseline was stabilized by performing 2–5 startup cycles, where each cycle includes a capture and a regeneration step. The capture step was performed by an injection of a total of 10–25 ng transcribed cis-blocked RNA diluted in HBS-N buffer over the reaction flow cell (FC2) for 1 min at a flow rate of 10 µl/min. The capture step typically yielded ~50–300 RU of the SPR signal for the described constructs. The regeneration step was performed by an injection of 25 mM NaOH over both flow cells for 30 sec at a flow rate of 30 µl/min.

Following the startup cycles, assay cycles were performed. Each assay cycle includes a capture, a reaction and a regeneration step. The capture and regeneration steps in an assay cycle were performed as described for those in the startup cycle. The reaction step was performed by an injection of the running buffer containing 500 µM $MgCl_2$ with or without 5 mM theophylline over both FCs for 5 min at a flow rate of 10 µl/min. Biacore sensorgram processing and analysis were performed using Biacore X100 Evaluation Software v2.0 (Biacore). Due to the slight time delay at which injected analyte reaches the respective flow cells, the resultant sharp spikes at the beginning and the end of injection were excluded from the analysis (18). The processed sensorgram (R) was fit to a simple exponential equation $R = (R_0 - R_\infty) \times (e^{-kdt}) + R_\infty$, where R_0 (fit globally for a given replicate) is the initial SPR signal before the cleavage reaction, R_∞ (fit locally for a given replicate) is the residual response at the end of the cleavage reaction and kd is the first-order RNA dissociation rate constant. Reported values are the mean of at least three independent experiments.

RESULTS

A cis-acting RNA blocking sequence allows inhibition of ribozyme cleavage during transcription

To prevent ribozyme constructs from cleaving during transcription, we developed a new blocking method to inhibit the formation of ribozyme-active conformations co-transcriptionally. This blocking method was initially demonstrated for the type III HHRz (with 5′ and 3′ termini in stem III) from sTRSV (Figure 2A). We rationally designed a 12-nt RNA blocking sequence that is complementary to part of the sTRSV HHRz transcript (Figure 2B). The RNA blocking sequence was inserted at the 5′ end of the sTRSV HHRz transcript to generate a cis-blocked sTRSV HHRz construct. As the RNA is being synthesized, the blocking sequence is capable of competitively hybridizing to the targeted ribozyme sequence, thus preventing the transcribed RNA from adopting a ribozyme-active conformation (Figure 2B).

A trans-acting DNA activator allows release of blocked RNA through a strand-displacement reaction

To activate the blocked sTRSV HHRz RNA for subsequent cleavage assays, we rationally designed a 10-nt RNA activation sequence as a single-stranded domain directly attached to the 5′ end of the RNA blocking sequence (Figure 2B). The RNA activation sequence serves as a toehold to allow for the design of a 21-nt DNA activator complementary to the RNA activation sequence and the first 11 nt of the RNA blocking sequence (Figure 2C). A toehold length between 5–10 nt has been demonstrated to enhance the rate of strand-displacement reactions by ~10^6-fold (19). In this way, the DNA activator can sequester the RNA blocking sequence through a rapid toehold-mediated strand-displacement reaction, thus allowing the RNA to adopt the ribozyme-active conformation in the presence of DNA activator for subsequent cleavage assays.

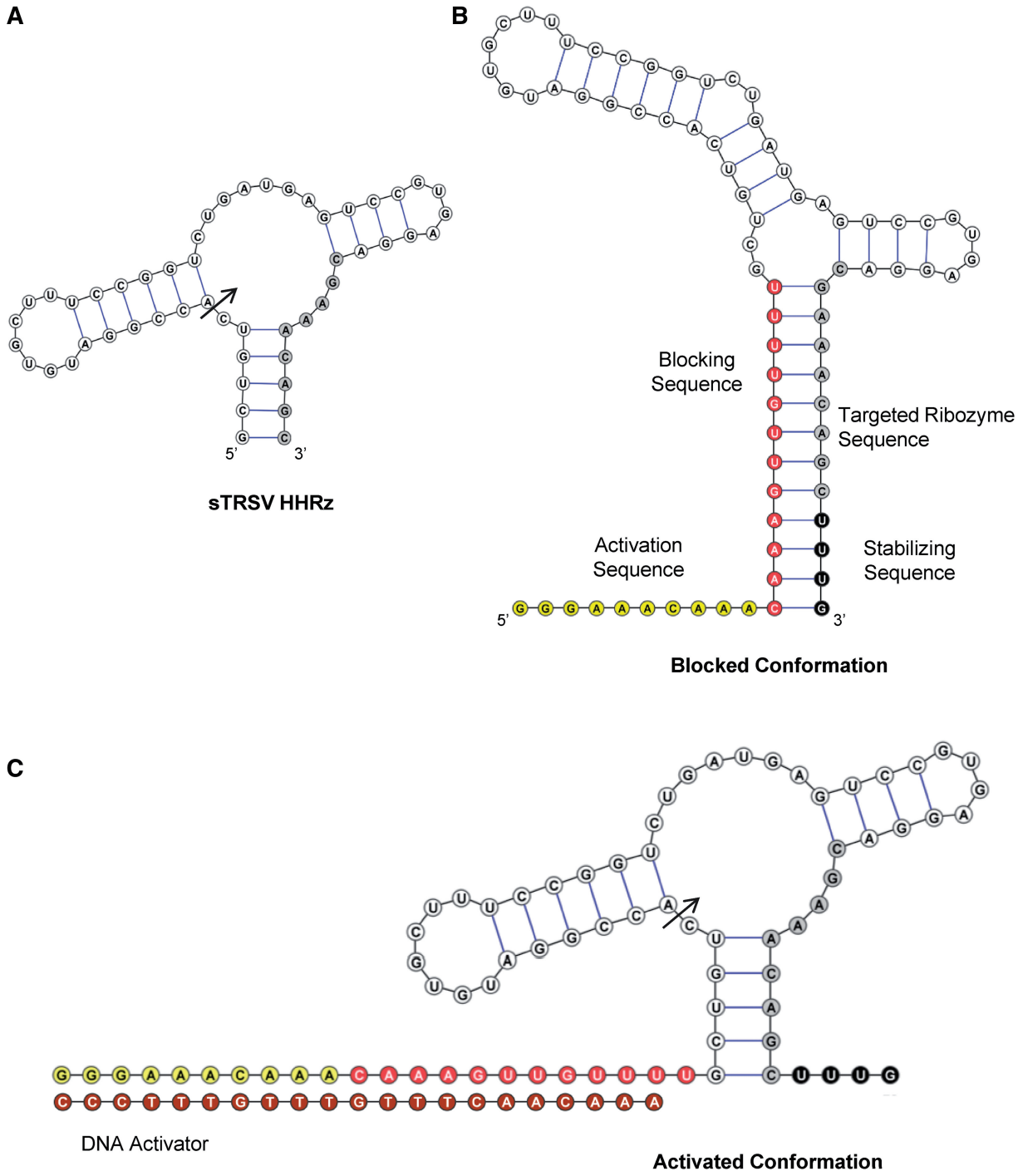

Figure 2. Development of a cis-blocking and trans-activation strategy to generate functional continuous ribozyme-encoding RNA through *in vitro* transcription reactions. (**A**) The cis-blocking strategy is illustrated on the sTRSV HHRz, and the arrow indicates the location of the cleavage site. (**B**) A cis-blocking method can block the folding of a transcript into a ribozyme-active conformation. An RNA blocking sequence (red), complementary to part of the ribozyme (targeted ribozyme sequence, grey), is directly incorporated into the 5′ end of the ribozyme-encoding transcript and inhibits the ribozyme construct from folding into the active conformation during the transcription reaction. The activation sequence (yellow) provides a toehold for the DNA activator strand, and the stabilizing sequence (black) can be modified to alter the length of the toehold and the stability of the cis-blocked conformation. (**C**) A trans-activation method can redirect the folding of a cis-blocked transcript into a ribozyme-active conformation. The cis-blocked ribozyme construct can be relieved by the addition of a DNA activator strand (brown), which competes with the targeted ribozyme sequence for binding to the blocking sequence through a toehold-mediated strand-displacement reaction. As shown here, hybridization between the ribozyme-encoding transcript and the DNA activator results in the transcript adopting the ribozyme-active conformation. All secondary structures were predicted by RNAstructure folding software (32) and rendered using VARNA software (33).

A RNA stabilizing sequence allows tuning of blocking efficiency

We tuned the strength of the competitive hybridization interaction between the RNA blocking and targeted ribozyme sequences by introducing a stabilizing sequence at the 3′ end of the cis-blocked sTRSV HHRz construct (Figure 2B). The stabilizing sequence is designed to hybridize to the RNA activation sequence such that the thermal stability of the blocked conformation can be tuned by varying the length of the stabilizing sequence. We increased the length of the stabilizing sequence from 4 to 14 nt in steps of 2 nt to generate a variety of cis-blocked sTRSV HHRz constructs (Supplementary Figure S1). The blocking efficiencies of the resultant sTRSV HHRz variants were determined by quantifying the fraction uncleaved RNA through PAGE analysis on the transcription products (Figure 3A). By adding 2 nt to the originally designed stabilizing sequence (sTRSV-2 HHRz construct), we increased the blocking efficiency from ~44% to ~93%. These results support that the cis-blocking method is efficient in inhibiting ribozyme cleavage during transcription.

We next incubated the cis-blocked sTRSV HHRz variants at 5 mM $MgCl_2$, a concentration at which the sTRSV HHRz is expected to undergo complete cleavage within seconds (12). We observed no cleavage even after a prolonged incubation time (1 h), indicating that the RNA was incapable of spontaneously releasing itself from the blocked conformation (Figure 3A). We then examined the efficacy of the toehold-mediated trans-activation strategy by incubating the constructs at the same $MgCl_2$ concentration in the presence of the activator strand. The activation efficiencies of the cis-blocked constructs were determined by quantifying the fraction cleaved of the blocked RNA through PAGE analysis at the end of incubation. By simple mixing of the cis-blocked constructs and the activator strand without any denaturation and refolding steps, we observed activation efficiencies up to ~88% of the blocked RNA (Figure 3A). The extent of cleavage decreased as the toehold length decreased, and the data indicate that the rate of the strand displacement reaction may be too slow to allow effective activation of the blocked RNA with toehold lengths between 0 and 2 nt. These results highlight that our two-step cis-blocking and trans-activation strategy can be tuned to efficiently generate full-length functional RNA. The cis-blocked sTRSV-2 HHRz construct was chosen for further characterization owing to its high blocking and activation efficiencies.

The cis-blocking mechanism provides a modular strategy for inhibiting cleavage of various types of HHRzs

To examine the flexibility of our two-step strategy, we applied the cis-blocking and trans-activation methods to the generation of functional continuous RNA for other natural HHRzs. We initially tested the HHRz from the peach latent mosaic viroid RNA (pLMVd), which exhibits the same type III topology as the sTRSV HHRz (20) (Supplementary Figure S2A). The RNA blocking, activation and DNA activator sequences designed for the sTRSV HHRz were modified for complementarity to the pLMVd HHRz sequence (Supplementary Figure S2B). The blocking and activation efficiencies were assayed under the same incubation conditions as for the cis-blocked sTRSV HHRz constructs (Figure 3B). The cis-blocked pLMVd HHRz RNA exhibited a blocking efficiency of ~80% and an activation efficiency of ~55%. The observed final fraction of cleaved cis-blocked pLMVd HHRz RNA is in agreement with the previously reported fraction of cleaved wild-type pLMVd HHRz measured at the end of a cleavage reaction (21).

Next, we applied the two-step cis-blocking and trans-activation strategy to HHRzs that exhibit the type I topology (with 5′ and 3′ termini in stem I) (Supplementary Figure S2A). We designed the RNA blocking sequences to target the catalytic core region connecting stems I and II of the HHRz encoded by the wild-type satellite DNA of *Schistosoma mansoni* HHRzs (22) and an evolved *S. mansoni* HHRz variant (Smα1-CG HHRz) that exhibits improved cleavage kinetics (21) (Supplementary Figure S2C and D). Stabilizing sequences were omitted from these cis-blocked constructs, as the blocked conformations were predicted to be relatively stable without them. Both cis-blocked *S. mansoni* and Smα1-CG HHRz constructs exhibited high blocking efficiencies of ~98% and ~81%, respectively (Figure 3B). However, the activation efficiency of the cis-blocked *S. mansoni* HHRz RNA (~24%) was significantly lower than that of the cis-blocked Smα1-CG HHRz RNA (~78%) (Figure 3B). Relatively poor cleavage activity of the *S. mansoni* HHRz has been previously observed and attributed to inactive/alternate RNA conformations (23). Improved cleavage activity has been observed for this ribozyme when assays were performed at different conditions (14,24). By varying the $MgCl_2$ concentration, incubation temperature and incubation time, we improved the activation efficiency of the cis-blocked *S. mansoni* HHRz RNA from ~24% to ~74% (Supplementary Figure S3).

The sTRSV-blocking sequence provides a modular strategy for inhibiting cleavage of sTRSV ribozyme-based devices

The designed RNA blocking sequence for the sTRSV HHRz targets a region within the ribozyme, and thus we anticipate that the strategy developed for the sTRSV HHRz can be directly applied to generate full-length RNA for sTRSV HHRz-based devices (3,25). We inserted the RNA blocking and activation sequences in a series of previously characterized ribozyme devices composed of different sensor, transmitter and actuator components to generate the corresponding cis-blocked L2b1, L2b5, L2b8, L2b8-a1, L2b8-a14, L2b8-a1-t41, L2bOFF1 and L2b8tc constructs (25) (Supplementary Figure S4). All synthetic devices described here were designed to respond to theophylline, except for the L2b8tc device, which was designed to respond to tetracycline. The blocking and activation efficiencies for all ribozyme devices were assayed under the same conditions as for the cis-blocked sTRSV HHRz RNA (Figure 3C). Blocking efficiencies of up to ~92% were obtained, supporting that the RNA

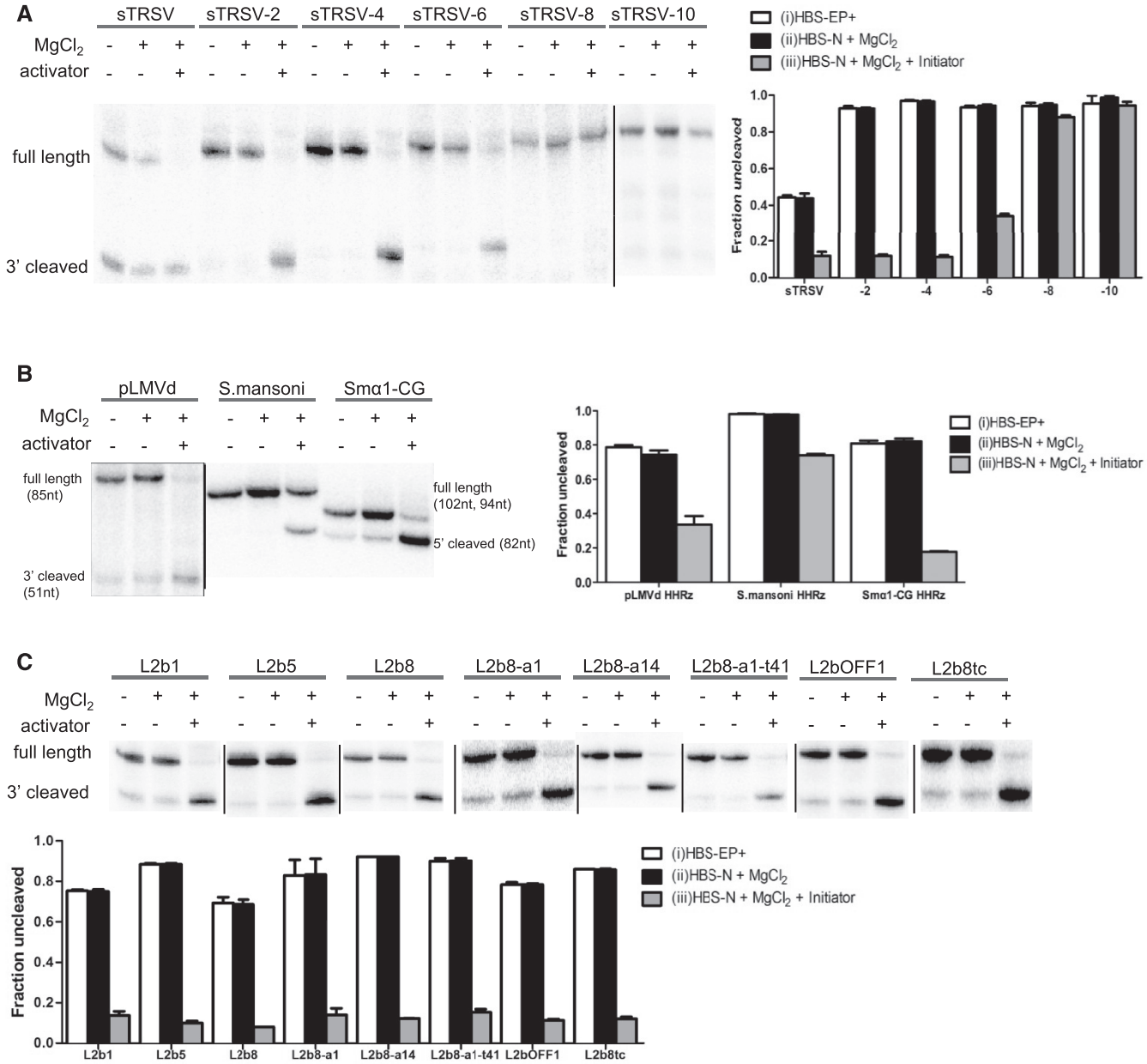

Figure 3. The cis-blocking and trans-activation strategy supports efficient blocking and activation of diverse ribozyme-encoding transcripts. (**A**) The toehold length tunes the efficiency of blocking and activation through the cis-blocking and trans-activation strategy applied to the wild-type sTRSV HHRz. Cis-blocked sTRSV HHRz construct variants were incubated in the following: (i) HBS-EP buffer (10 mM HEPES, 150 mM NaCl, 3 mM EDTA, 0.05% P20, pH 7.4) (first lane); (ii) HBS-N buffer (10 mM HEPES, 150 mM NaCl, pH 7.4) in the presence of 5 mM $MgCl_2$ for 1 h at 25°C (second lane); and (iii) HBS-N buffer in the presence of 5 mM $MgCl_2$ and 10 μM activator for 1 h at 25°C (third lane) (top panel). Denaturing PAGE was used to separate the products from the transcription and cleavage reactions, where uncleaved and 3′ cleaved fragments are shown. The fraction RNA cleaved for each incubation condition was quantified by autoradiography (bottom panel). (**B**) The two-step cis-blocking and trans-activation strategy can be applied to HHRz variants exhibiting diverse topologies and sequences. Cis-blocked constructs of the pLMVd HHRz, *S.mansoni* HHRz and an evolved *S. mansoni* HHRz variant (Smα1-CG HHRz) were constructed and analysed in same manner as the sTRSV HHRz in Figure 3A. (**C**) The two-step cis-blocking and trans-activation strategy can be directly applied to synthetic ribozyme devices. The blocking and activation sequences designed for the sTRSV HHRz were directly incorporated into various synthetic ribozyme devices (L2b1, L2b5, L2b8, L2b8-a1, L2b8-a14, L2b8-a1-t41, L2bOFF1, L2b8tc). The ribozyme device transcription products were analysed as described for the cis-blocked sTRSV HHRz constructs in Figure 3A. A black vertical bar was used to denote samples run on different gels.

blocking sequence is modular to constructs encoding ligand-responsive ribozymes based on the same ribozyme sequence. In contrast, performing transcription reactions on these devices in the absence of the cis-blocking sequence results in substantial cleavage of the ribozyme device-encoding transcripts (Supplementary Figure S5). The cis-blocked device transcripts were also incubated at 5 mM $MgCl_2$ in the absence and presence of the activator strand for an hour at 25°C (Figure 3C). Similar to the results with the HHRz alone, the cis-blocked ribozyme

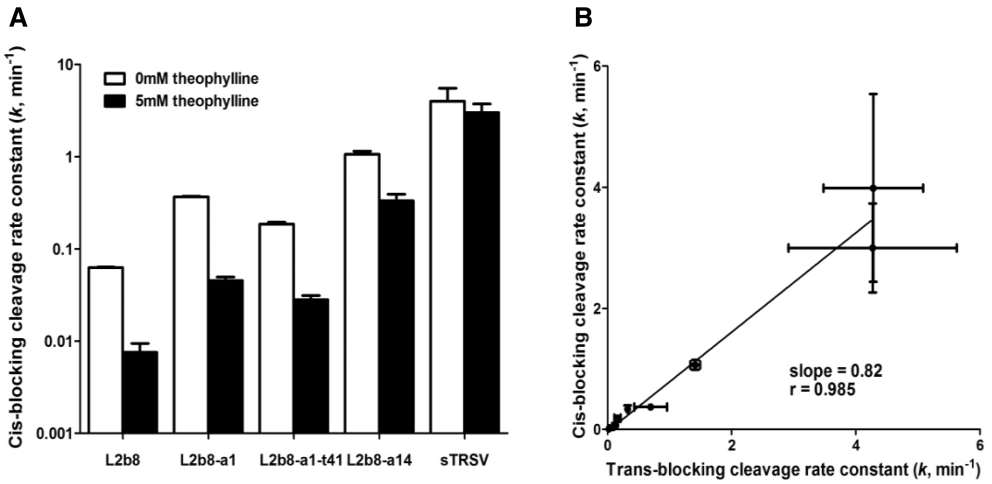

Figure 4. The two-step cis-blocking and trans-activation strategy does not impact the cleavage rate constants of the resulting ribozyme constructs. (**A**) *In vitro* ribozyme cleavage rate constants on full-length RNA generated from the cis-blocking strategy. Gel-based cleavage assays were performed on the cis-blocked sTRSV HHRz, L2b8, L2b8-a1, L2b8-a14 and L2b8-a1-t41 constructs at 37°C in 500 μM $MgCl_2$, 100 mM NaCl, 50 mM Tris-HCl (pH 7.5). Cleavage rate constants (k) and errors are reported as the mean and standard deviation from at least three independent assays. (**B**) Correlation analysis of cleavage rate constants of full-length RNA generated from the two ribozyme-encoding RNA generation strategies indicates a strong correlation between these two cleavage rate constants; Pearson correlation coefficient (r): 0.985, slope: 0.821 ± 0.05. The cleavage rate constants in the absence and presence of 5 mM theophylline for the sTRSV HHRz (4.3, 4.3 min^{-1}), L2b8-a14 (1.4, 0.33 min^{-1}), L2b8-a1 (0.7, 0.1 min^{-1}), L2b8-a1-t41 (0.16, 0.096 min^{-1}) and L2b8 (0.14, 0.025 min^{-1}) constructs were previously determined with the trans-blocking strategy under the same reaction conditions (25).

device transcripts require the presence of both $MgCl_2$ and DNA activator to cleave. Activation efficiencies of up to ~89% were obtained, supporting that the activator sequence optimized for the sTRSV HHRz can also be directly applied to the corresponding ribozyme devices.

Full-length RNA generated through the two-step, gel-free strategy exhibit similar cleavage rate constants to RNA generated through trans-blocking, gel-purified methods

We next examined the cleavage rate constants (k) measured for the functional continuous RNA generated through the two-step cis-blocking and trans-activation strategy. Gel-based cleavage assays were performed on radiolabeled transcripts at physiologically relevant reaction conditions [500 μM $MgCl_2$, 100 mM NaCl, 50 mM Tris-HCl (pH 7.5)] at 37°C (Supplementary Figure S6). The cis-blocked RNA was activated by incubation with the DNA activator strand for 1 min before the addition of $MgCl_2$. The cleavage rate constants were obtained for the cis-blocked sTRSV-2 HHRz (4.0, 3.0 min^{-1}), L2b8-14 (1.06, 0.33 min^{-1}), L2b8-a1 (0.351, 0.043 min^{-1}), L2b8-a1-t41 (0.186, 0.028 min^{-1}) and L2b8 (0.063, 0.008 min^{-1}) constructs in the absence and presence of 5 mM theophylline, respectively (Figure 4A). The cleavage rate constants measured for the cis-blocked sTRSV HHRz construct were comparable in the absence and presence of theophylline, indicating that theophylline has no non-specific effect on the cleavage activity. On the other hand, the cleavage rate constants measured for the synthetic ribozyme devices in the presence of theophylline were slower than those measured in the absence of theophylline, indicating that theophylline binding to the aptamer shifts the distribution between the two functional conformations to the ribozyme-inactive state and thus results in a slower cleavage activity as expected. We compared these rate constants with those previously obtained through the traditional trans-blocking strategy, which requires PAGE purification to recover the blocked full-length RNA strands (25) (Figure 4B). The measured cleavage rate constants through the two different ribozyme-encoding RNA generation strategies exhibit a strong linear correlation [Pearson product moment (r): 0.985] with a slope of 0.82. These results validate that the cis-blocking and trans-activation mechanisms used in our strategy have little impact on the measured ribozyme cleavage kinetics.

A label-free, continuous, SPR-based assay to support rapid monitoring of ribozyme cleavage

Our two-step cis-blocking and trans-activation strategy allows the development of a label-free, continuous cleavage assay based on the Biacore sensor platform (Figure 5). We generated a reaction sensor surface by covalently linking the DNA activator strand to the sensor surface (Figure 5A). The reaction sensor surface then allows both the capture and activation of the cis-blocked RNA through the programmed hybridization interaction (Figure 5B). The capture of RNA is monitored in real time and represented as an increase in the SPR signal owing to increased mass density near the sensor surface. The cleavage reaction is initiated by the injection of a buffer containing $MgCl_2$ across the flow cell surface (Figure 5C). Cleavage of the RNA results in a 3′ cleaved fragment that is weakly hybridized to the immobilized DNA activator strand through five bases, and the 3′ cleaved fragment dissociation rate constant can be predicted by a previously developed secondary structure nearest neighbor analysis (23) (Supplementary Figure S7). The predicted dissociation

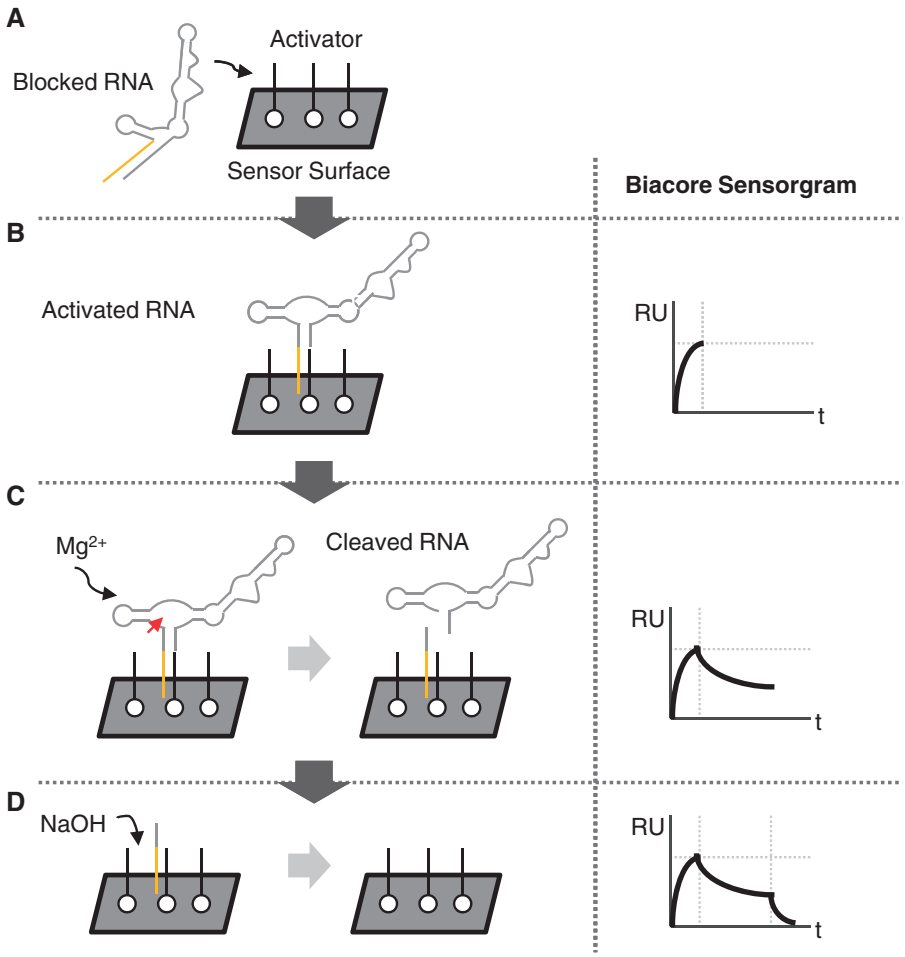

Figure 5. Schematic of the SPR-based ribozyme cleavage assay. (**A**) A sensor surface for ribozyme cleavage characterization is generated by conjugating the DNA activator strand directly to the chip surface. (**B**) The cis-blocked ribozyme-encoding transcript is injected over the activator-coated surface, and the hybridization interaction between the transcript and the activator strand results in an increase in SPR signal, represented by RU. The hybridization of the ribozyme construct to the activator-coated surface results in the RNA adopting the ribozyme-active conformation. (**C**) The cleavage reaction is initiated by the injection of buffer containing $MgCl_2$ over the sensor surface. Ribozyme cleavage results in a quick dissociation of the 3′ cleaved fragment, resulting in a decrease in SPR signal. The RNA dissociation rate constant is obtained by fitting the injection portion of the sensorgram to a first-order exponential decay equation (see Materials and Methods). (**D**) Finally, the surface is regenerated for the next assay by an injection of 25 mM NaOH to remove residual RNA.

rate constant is several orders of magnitude greater than the cleavage rate constant measured for the fastest cleaving construct in this study. Therefore, upon cleavage, the 3′ cleaved fragment will rapidly dissociate from the 5′ cleaved fragment-DNA activator duplex, resulting in a decrease in the SPR signal owing to decreased mass density near the sensor surface. The rate of SPR signal decrease, which reflects how fast the ribozyme construct cleaves, is fitted to a first-order exponential decay equation to obtain the RNA dissociation rate constant. During the assay, both full-length and 5′ cleaved fragments can also spontaneously dissociate, although slowly, from the activator strands and contribute to the observed decrease in SPR signal. Thus, the measured RNA dissociation rate constant is a lump sum of dissociation rate constants due to irreversible cleavage and reversible hybridization reactions. Lastly, because the DNA-based reaction sensor surface is highly stable, the surface can be regenerated, by an injection of nucleic acid denaturants (i.e. NaOH) to remove residual RNA, and reused for subsequent cleavage assays (Figure 5D).

The SPR-based RNA dissociation rate constants reflect the gel-based cleavage rate constants

The SPR-based cleavage assay was applied to monitor the cleavage of a set of cis-blocked ribozyme constructs under reaction conditions similar to the gel-based cleavage assay conditions. The cis-blocked sTRSV-2 HHRz and a series of cis-blocked ribozyme device (L2b8, L2b8-a1, L2b8-a14 and L2b8-a1-t41) transcripts were captured on the chip surface through the DNA activator. Cleavage reactions were subsequently initiated by injecting buffer [100 mM NaCl, 50 mM Tris-HCl (pH 8.5)] containing either (i) no $MgCl_2$, (ii) 500 μM $MgCl_2$, or (iii) 500 μM $MgCl_2$ and 5 mM theophylline (Figure 6A; Supplementary Figure S8). RNA dissociation rate constants were determined by fitting the resulting Biacore sensorgrams to a simple exponential equation.

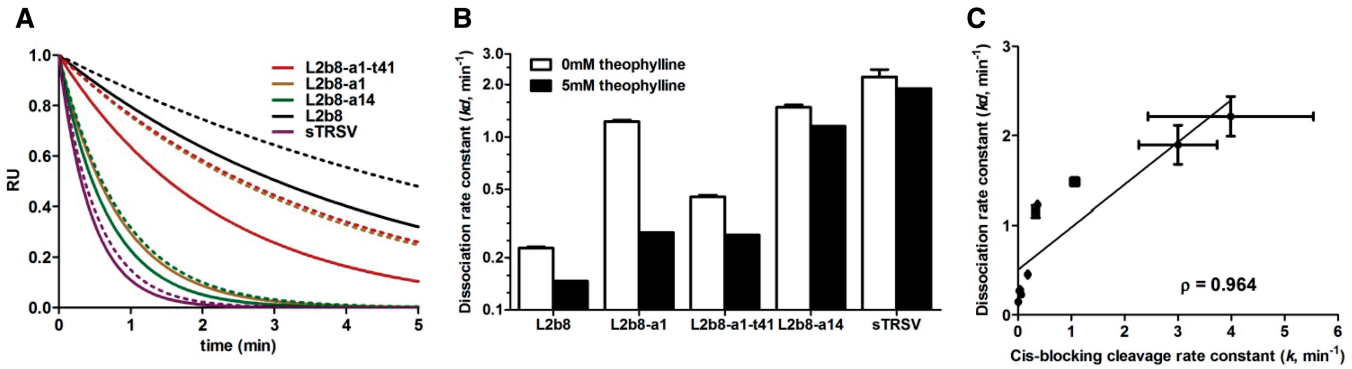

Figure 6. The SPR-based RNA dissociation rate constants are correlated to the corresponding gel-based cleavage rate constants. The SPR-based assays were performed on the cis-blocked sTRSV HHRz, L2b8, L2b8-a1, L2b8-a14 and L2b8-a1-t41 constructs at 37°C with buffer [100 mM NaCl, 50 mM Tris-HCl (pH 8.5)] containing the following: (i) 500 μM $MgCl_2$, (ii) 500 μM $MgCl_2$ and 5 mM theophylline. (**A**) The projected dissociation kinetics are generated from the single-exponential equation, $R = (R_0 - R_\infty) \times (e^{-kdt}) + R_\infty$, setting the SPR signal before the start of reaction (R_0) and residual response at the end of the cleavage reaction (R_∞) to 1 and 0, respectively, and *kd* to the experimentally determined value for each RNA device. Solid lines: 0 mM theophylline; dashed lines: 5 mM theophylline. (**B**) RNA dissociation rate constants (*kd*) and errors are reported as the mean and standard deviation from at least three independent assays. (**C**) Correlation analysis of observed RNA dissociation rate constants and corresponding ribozyme cleavage rate constants indicates a strong correlation between these two rate constants [Spearman (rank) correlation coefficient (ρ): 0.964].

The RNA dissociation rate constants due to ribozyme-independent spontaneous dissociation from the DNA activator are determined at reaction condition (i), as the ribozyme constructs are expected to exhibit little catalytic activity in the absence of $MgCl_2$ (26). The measured RNA dissociation rate constants at this condition range from 0.03 to 0.21 min^{-1}, suggesting that the reversible hybridization reaction exhibits a slow dissociation rate constant (Supplementary Figure S8). We next examined the RNA dissociation rate constants obtained under reaction conditions (ii) and (iii) (Figure 6B). For all theophylline-responsive ribozyme devices, the measured RNA dissociation rates in the presence of 5 mM theophylline are lower than the respective rates measured in the absence of theophylline, identical to the trend observed for the gel-based cleavage rate constants (Figure 4A). Theophylline binding to the aptamer component within the device is expected to result in no detectable change in SPR signal due to the low density of RNA being captured on the surface. In addition, the measured dissociation rate constants for the cis-blocked sTRSV-2 HHRz RNA are similar in the presence and absence of theophylline (1.9 and 2.2 min^{-1}, respectively), indicating that theophylline has little non-specific effect on the measured dissociation rate constants on the Biacore. We further characterized the dissociation rate constants of two of the ribozyme devices under different pH and magnesium ion concentrations and observed similar trends as expected from previous kinetics studies on the sTRSV HHRz (22,24,27–29) (Supplementary Figure S9).

Finally, we performed a ranking correlation analysis by comparing the cis-blocked ribozyme SPR-based RNA dissociation rate constants to the corresponding gel-based cleavage rate constants. The rate constants obtained through the two different characterization methods show a significant statistical dependence, with a high Spearman (rank) correlation coefficient ($\rho = 0.964$) (Figure 6C). These results support that the SPR-based RNA dissociation rate constant reflects the ribozyme cleavage rate constant. However, the dissociation rate constants determined by the SPR-based assay become less reflective of the cleavage activities when characterizing ribozyme constructs that exhibit slow cleavage kinetics. For example, the RNA dissociation rate constant for the L2b8 construct in the presence of theophylline, which exhibits the slowest cleavage rate constant (0.15 min^{-1}) among the ribozyme constructs characterized, is comparable with that in the absence of $MgCl_2$ (0.08 min^{-1}), suggesting that the measured rate constant is largely contributed to by the cleavage-independent dissociation reaction.

DISCUSSION

We developed an efficient two-step ribozyme blocking and activation strategy that supports scalable generation of functional continuous transcripts encoding ribozyme constructs through *in vitro* transcription reactions. Our strategy is inspired by the natural cis-blocking mechanism used by the HDV ribozyme (16). We developed a similar cis-blocking method by designing a synthetic RNA blocking sequence complementary to the 3′ end of the HHRz to prevent the formation of the active HHRz structure during transcription. We demonstrated a tuning strategy based on stabilizing the blocked HHRz conformation to increase blocking efficiency. As our strategy depends on the addition of independent blocking sequences flanking the ribozyme sequence, these added sequences can be readily altered to work with a variety of different ribozyme sequences and architectures. The adaptability and broad utility of our strategy was demonstrated on additional type I and type III HHRzs and a wide array of synthetic ribozyme devices.

Previous kinetic studies demonstrated that ~50% of the full-length RNA generated by the trans-blocking strategy remains uncleaved (8). We speculate that the use of a

denaturing PAGE purification step for the recovery of full-length transcription products, which requires an additional RNA refolding step, may render the trans-blocking method more prone to misfolding and therefore result in significant amounts of inactive transcription products. We used a trans-activation method based on a toehold-mediated strand-displacement mechanism, which offers the advantage of bypassing the need of additional RNA denaturation and refolding steps, thus providing a rapid two-step process (co-transcriptional blocking and activation) to yield large quantities of functional continuous RNA without the need of laborious PAGE purification processes. Kinetic assays demonstrated that the *in vitro* cleavage rate constants measured for ribozymes generated through our two-step cis-blocking and trans-activation strategy were similar to those rate constants measured for identical ribozymes generated through the more traditional trans-blocking and gel purification method, supporting that our strategy minimally impacts the resulting ribozyme cleavage kinetics. This is in contrast to a trans-activation method previously used in the development of allosteric HHRz targeted ribozyme-attenuated probes (TRAP) (10), in which an attenuation probe was appended to the 3′ end of the enzyme strand of a discontinuous HHRz and designed to anneal to the catalytic core, thus inhibiting cleavage of the substrate strand. The blocked HHRz was released by denaturing and refolding the enzyme and substrate strands with an antisense strand designed to sequester the attenuation probe. Slower measured cleavage rate constants were observed for the activated TRAP system, suggesting that the hybridization reaction between the antisense strand and attenuation probe is kinetically limited.

Our strategy uses a trans-acting DNA strand to activate the blocked RNA, supporting the development of a novel cleavage assay based on SPR. Our SPR-based assay offers several unique advantages over the more traditional gel-based assay, in that it allows label-free, real-time and continuous monitoring of ribozyme cleavage. In addition, the SPR instrument requires little material due to a microfluidics-based flow system and is highly automatable to support scalable characterization of many different ribozyme constructs. The SPR-based cleavage assay was applied to measure the rate constant of SPR signal decrease for a set of ribozyme-encoding transcripts under physiologically relevant conditions. The results of a rank correlation analysis support that the measured RNA dissociation rate constants from our SPR-based assays reflect the ribozyme cleavage rate constants obtained from the gel-based assays. However, there is an inherent limitation in the SPR assay, which is based on linking a chemical reaction step to a product dissociation event. Under certain reaction conditions (e.g. high Mg concentrations at which ribozymes exhibit high cleavage activity) the product dissociation may become the rate-limiting step. In this case, the measured RNA dissociation rate constant will be largely determined by the product dissociation rate constant and thus provides little information on the actual ribozyme cleavage activity.

Another limitation in our current assay design is that the measured RNA dissociation rate constant is contributed to by both the cleavage-dependent dissociation rate constant (3′ cleaved fragment from the 5′ cleaved fragment-immobilized DNA activator hybrid) and cleavage-independent dissociation rate constant (5′ cleaved and full-length fragments from the immobilized DNA activator). In the case of constructs that exhibit a slow chemical step (with a rate constant comparable with that of the cleavage-independent dissociation step), the measured RNA dissociation rate constant can be significantly contributed to by the cleavage-independent dissociation rate constant. In other words, the measured RNA dissociation rate will reflect the chemical step less and thus provide little information on ribozyme cleavage activity. In addition, the format of any SPR-based assay requires continuous injection of analytes, which presents limitations for the characterization of ribozyme constructs exhibiting low cleavage activities (and thus requiring longer injection times). To address these limitations, efforts can be directed toward enhancing the stability of the hybridization reaction between the ribozyme-encoding RNA and the DNA activator. For example, the length of the RNA activation sequence can be extended or alternative backbones for the activator strand, such as peptide nucleic acid, can be used that will result in more stable duplexes with the RNA transcript (30). As an additional approach, the range of cleavage activities that can be analysed through the SPR-based assays may be extended by using instrument platforms that support analysis over longer reaction times. For example, an instrument can be set up to inject analyte directly through the running buffer syringe or the instrument can be modified with an external peristaltic pump (31). With further development, our SPR-based cleavage assay will offer a powerful strategy for rapid, quantitative characterization of a wide variety of ribozyme constructs.

Recent advances in RNA engineering have successfully coupled ribozymes to various natural and synthetic sensor components to construct gene-regulatory devices that function in diverse genetic systems (3–6). We have previously demonstrated that the *in vitro* cleavage rate constants and *in vivo* gene-regulatory activities of these ribozyme-based devices are closely correlated (25). In addition, recent computational models have highlighted the direct and multi-faceted impact that cleavage rate constants can have on the *in vivo* gene-regulatory performance of this class of genetic devices, supporting this property as a key engineering parameter to target for device optimization (7). Therefore, enabling tools that support rapid and scalable functional characterization of ribozyme constructs will advance our ability to characterize key properties of these genetic devices (e.g. *in vitro* cleavage rate constants) and thus guide the design of new ribozyme-based devices with improved gene-regulatory activities. The described two-step ribozyme cis-blocking and trans-activation strategy provides an efficient, scalable method for generating continuous ribozyme-encoding transcripts for further downstream characterization. This approach is fully complemented by the rapid, label-free and real-time SPR-based cleavage assay, which directly integrates the trans-activation strategy with the recruitment step to the chip surface. Together, these

methods describe a streamlined, solution-based strategy for ribozyme device characterization that will support the design, optimization and probing of this important class of regulatory molecules.

SUPPLEMENTARY DATA

Supplementary Data are available at NAR Online: Supplementary Table 1, Supplementary Figures 1–9 and Supplementary References [3,22,24,25,27–29,32–36].

ACKNOLEDGEMENTS

The authors thank J. Schuman of GE and M. Eckhart of the Stanford PAN facility. A.B.K. and J.C.L. designed research, performed research and wrote the article; C.D.S. designed research and wrote the article.

FUNDING

The National Institutes of Health [R01GM086663]; the National Science Foundation [CBET-0917638, CCF-0943269]; the Defense Advanced Research Projects Agency [HR0011-11-2-0002]; the National Sciences and Engineering Research Council of Canada (fellowship to A.B.K.). Funding for open access charge: the Defense Advanced Research Projects Agency.

Conflict of interest statement. The authors declare competing financial interests in the form of a pending patent application.

REFERENCES

1. Nandagopal,N. and Elowitz,M.B. (2011) Synthetic biology: integrated gene circuits. *Science*, **333**, 1244–1248.
2. Liang,J.C., Bloom,R.J. and Smolke,C.D. (2011) Engineering biological systems with synthetic RNA molecules. *Mol. Cell*, **43**, 915–926.
3. Win,M.N. and Smolke,C.D. (2007) A modular and extensible RNA-based gene-regulatory platform for engineering cellular function. *Proc. Natl Acad. Sci. USA*, **104**, 14283–14288.
4. Chen,Y.Y., Jensen,M.C. and Smolke,C.D. (2010) Genetic control of mammalian T-cell proliferation with synthetic RNA regulatory systems. *Proc. Natl Acad. Sci. USA*, **107**, 8531–8536.
5. Wieland,M. and Hartig,J.S. (2008) Improved aptazyme design and in vivo screening enable riboswitching in bacteria. *Angew. Chem. Int. Ed. Engl.*, **47**, 2604–2607.
6. Win,M.N. and Smolke,C.D. (2008) Higher-order cellular information processing with synthetic RNA devices. *Science*, **322**, 456–460.
7. Beisel,C.L. and Smolke,C.D. (2009) Design principles for riboswitch function. *PLoS Comput. Biol.*, **5**, e1000363.
8. Nelson,J.A., Shepotinovskaya,I. and Uhlenbeck,O.C. (2005) Hammerheads derived from sTRSV show enhanced cleavage and ligation rate constants. *Biochemistry*, **44**, 14577–14585.
9. Mercure,S., Lafontaine,D., Ananvoranich,S. and Perreault,J.P. (1998) Kinetic analysis of delta ribozyme cleavage. *Biochemistry*, **37**, 16975–16982.
10. Burke,D.H., Ozerova,N.D. and Nilsen-Hamilton,M. (2002) Allosteric hammerhead ribozyme TRAPs. *Biochemistry*, **41**, 6588–6594.
11. Stage-Zimmermann,T.K. and Uhlenbeck,O.C. (1998) Hammerhead ribozyme kinetics. *RNA*, **4**, 875–889.
12. Khvorova,A., Lescoute,A., Westhof,E. and Jayasena,S.D. (2003) Sequence elements outside the hammerhead ribozyme catalytic core enable intracellular activity. *Nat. Struct. Biol.*, **10**, 708–712.
13. Singh,K.K., Parwaresch,R. and Krupp,G. (1999) Rapid kinetic characterization of hammerhead ribozymes by real-time monitoring of fluorescence resonance energy transfer (FRET). *RNA*, **5**, 1348–1356.
14. Penedo,J.C., Wilson,T.J., Jayasena,S.D., Khvorova,A. and Lilley,D.M. (2004) Folding of the natural hammerhead ribozyme is enhanced by interaction of auxiliary elements. *RNA*, **10**, 880–888.
15. Rich,R.L., Papalia,G.A., Flynn,P.J., Furneisen,J., Quinn,J., Klein,J.S., Katsamba,P.S., Waddell,M.B., Scott,M., Thompson,J. *et al*. (2009) A global benchmark study using affinity-based biosensors. *Anal. Biochem.*, **386**, 194–216.
16. Chadalavada,D.M., Knudsen,S.M., Nakano,S. and Bevilacqua,P.C. (2000) A role for upstream RNA structure in facilitating the catalytic fold of the genomic hepatitis delta virus ribozyme. *J. Mol. Biol.*, **301**, 349–367.
17. Myszka,D.G. (2000) Kinetic, equilibrium, and thermodynamic analysis of macromolecular interactions with BIACORE. *Methods Enzymol.*, **323**, 325–340.
18. Myszka,D.G. (1999) Improving biosensor analysis. *J. Mol. Recognit.*, **12**, 279–284.
19. Zhang,D.Y. and Seelig,G. (2011) Dynamic DNA nanotechnology using strand-displacement reactions. *Nat. Chem.*, **3**, 103–113.
20. Hernandez,C. and Flores,R. (1992) Plus and minus RNAs of peach latent mosaic viroid self-cleave in vitro via hammerhead structures. *Proc. Natl Acad. Sci. USA*, **89**, 3711–3715.
21. Saksmerprome,V., Roychowdhury-Saha,M., Jayasena,S., Khvorova,A. and Burke,D.H. (2004) Artificial tertiary motifs stabilize trans-cleaving hammerhead ribozymes under conditions of submillimolar divalent ions and high temperatures. *RNA*, **10**, 1916–1924.
22. Ferbeyre,G., Smith,J.M. and Cedergren,R. (1998) Schistosome satellite DNA encodes active hammerhead ribozymes. *Mol. Cell Biol.*, **18**, 3880–3888.
23. Canny,M.D., Jucker,F.M. and Pardi,A. (2007) Efficient ligation of the Schistosoma hammerhead ribozyme. *Biochemistry*, **46**, 3826–3834.
24. Canny,M.D., Jucker,F.M., Kellogg,E., Khvorova,A., Jayasena,S.D. and Pardi,A. (2004) Fast cleavage kinetics of a natural hammerhead ribozyme. *J. Am. Chem. Soc.*, **126**, 10848–10849.
25. Liang,J.C., Chang,A.L., Kennedy,A.B. and Smolke,C.D. (2012) A high-throughput, quantitative cell-based screen for efficient tailoring of RNA device activity. *Nucleic Acids Res*, **40**, e154.
26. Curtis,E.A. and Bartel,D.P. (2001) The hammerhead cleavage reaction in monovalent cations. *RNA*, **7**, 546–552.
27. Murray,J.B., Dunham,C.M. and Scott,W.G. (2002) A pH-dependent conformational change, rather than the chemical step, appears to be rate-limiting in the hammerhead ribozyme cleavage reaction. *J. Mol. Biol.*, **315**, 121–130.
28. Roychowdhury-Saha,M. and Burke,D.H. (2006) Extraordinary rates of transition metal ion-mediated ribozyme catalysis. *RNA*, **12**, 1846–1852.
29. Buskiewicz,I.A. and Burke,J.M. (2012) Folding of the hammerhead ribozyme: pyrrolo-cytosine fluorescence separates core folding from global folding and reveals a pH-dependent conformational change. *RNA*, **18**, 434–448.
30. Jensen,K.K., Orum,H., Nielsen,P.E. and Norden,B. (1997) Kinetics for hybridization of peptide nucleic acids (PNA) with DNA and RNA studied with the BIAcore technique. *Biochemistry*, **36**, 5072–5077.
31. Navratilova,I., Eisenstien,E. and Myszka,D.G. (2005) Measuring long association phases using Biacore. *Anal. Biochem.*, **344**, 295–297.
32. Mathews,D.H., Disney,M.D., Childs,J.L., Schroeder,S.J., Zuker,M. and Turner,D.H. (2004) Incorporating chemical modification constraints into a dynamic programming algorithm for prediction of RNA secondary structure. *Proc. Natl Acad. Sci. USA*, **101**, 7287–7292.

33. Darty,K., Denise,A. and Ponty,Y. (2009) VARNA: Interactive drawing and editing of the RNA secondary structure. *Bioinformatics*, **25**, 1974–1975.
34. Turner,D.H. and Mathews,D.H. (2010) NNDB: the nearest neighbor parameter database for predicting stability of nucleic acid secondary structure. *Nucleic Acids Res.*, **38**, D280–D282.
35. Turner,D.H. (2000) Double Helix Formation by Oligonucleotides Without Loops. In: Bloomfield,V.A., Crothers,D.M. and Tinoco,I.J. (eds), *Nucleic Acids: Structures, Functions and Properties*. University Science Books, Sausalito, CA, pp. 271–287.
36. Hertel,K.J., Herschlag,D. and Uhlenbeck,O.C. (1994) A kinetic and thermodynamic framework for the hammerhead ribozyme reaction. *Biochemistry*, **33**, 3374–3385.